BNL-45750
Conf-900993--2

To be published in: Proceedings of the III International Conference on "Applications of Physics in Medicine and Biology". Trieste, Italy. September 4-7, 1990.

BNL--45750

DE91 008108

Multiple Energy Computed Tomography for Neuroradiology with Monochromatic X-Rays from the National Synchrotron Light Source

F. A. Dilmanian[1], R.F. Garrett[1], W.C. Thomlinson[2], L.E. Berman[2], L.D. Chapman[2], N.F. Gmür[2], N.M. Lazarz[2], P.N. Luke[3], H.R. Moulin[2], T. Oversluizen[2], D.N. Slatkin[1], V. Stojanoff[2*], A.C. Thompson[3], N.D. Volkow[1], and H.D. Zeman[2+]

[1]Medical Department, and [2]National Synchrotron Light Source, Brookhaven National Laboratory, Upton, NY 11973, USA
[3]Lawrence Berkeley Laboratory, Berkeley, CA 94720, USA
*Permanent address: Institute of Physics, Univ. of São Paolo, São Paolo, Brazil
+Current address: Department of Biomedical Engineering, Univ. of Tennessee, Memphis, TN 38163, USA

ABSTRACT

Monochromatic and tunable 33-100 keV x-rays from the X17 superconducting wiggler of the National Synchrotron Light Source (NSLS) at Brookhaven National Laboratory (BNL) will be used for computed tomography (CT) of the human head and neck. The CT configuration will be one of a fixed horizontal fan-shaped beam and a seated rotating subject. The system, which is under development, will employ a two-crystal monochromator with an energy bandwidth of about 0.1%, and a high-purity germanium linear array detector with 0.5 mm element width and 200 mm total width. Narrow energy bands not only eliminate beam hardening but are ideal for carrying out the following dual-energy methods: a) dual-photon absorptiometry CT, that provides separate images of the low-Z and the intermediate-Z elements; and b) K-edge subtraction CT of iodine and perhaps of heavier contrast elements. As a result, the system should provide ~10-fold improvement in image contrast resolution and in quantitative precision over conventional CT. A prototype system for a 45 mm subject diameter will be ready in 1991, which will be used for studies with phantoms and small animals. The human imaging system will have a field of view of 200 mm. The in-plane spatial resolution in both systems will be 0.5 mm FWHM.

I. INTRODUCTION

Monochromatic x-rays have two advantages over the wide-energy bremsstrahlung radiation obtained from x-ray tubes for radiology in general and for CT in particular. First, monochromatic x-rays do not undergo "beam hardening", an effect associated with x-rays with a wide-energy spectrum as they pass through the body [1]. The basis of the effect is that the low-energy end of the spectrum attenuates more than does the high-energy end, which shifts the mean energy of the spectrum towards higher energy. This effect is particularly detrimental to CT, since the beam-hardening errors in x-ray projections at different angles are combined during tomographic reconstruction. The result is a loss of image contrast and quantitative precision, as well as the development of image artifacts [1]. The other advantage of monochromatic x-rays is their applicability to the multiple-energy radiological methods of dual-photon absorptiometry (DPA) [2] and K-edge subtraction (KES) [3] with iodine or with a heavier contrast element. Conceivably, DPA CT with monochromatic x-rays should be the best possible high sensitivity quantitative CT (QCT) [4], while KES CT should also provide unprecedented sensitivity and quantitative precision for imaging with contrast agents.

X-ray tubes used in conventional CT systems cannot provide adequate flux for monochromatic CT. At present, only synchrotron radiation can provide the necessary intensity. This paper describes the design and potential clinical research applications of a multiple energy computed tomography (MECT) system being developed at the X17 superconducting wiggler beamline at the NSLS. Fig. 1 is a schematic top view of the MECT system. It uses a fixed fan-shaped beam with 5 milliradian horizontal and 0.2 milliradian vertical opening angles. Therefore, the horizontal beam width at the patient's position, 40 meters from the source, will be 200 mm, while the vertical beam height, adjustable with a slit, will range from 1 to 8 mm.

II. THEORY

A. Advantages of monochromatic x-rays for CT

A.1. The beam-hardening problem

The principal advantage of monochromatic x rays for CT is the elimination of beam hardening effects. In conventional CT, detrimental effects of beam hardening are partially alleviated in two ways: a) by narrowing the energy width of the bremsstrahlung radiation through beam filtration, as far as the intensity of the x-ray tube allows, producing an energy bandwidth of several tens of percent; and b) by using computer algorithms to compare the effect in the subject with that in a phantom [1]. Although more detailed corrections can be made using dual-energy methods [1,5], in principle no correction will provide the excellent image quality foreseen with monochromatic x-rays .

A.2. Dual Photon Absorptiometry (DPA) CT

DPA is an imaging method in which the attenuation of x-rays at two greatly different energies (such as 40 and 100 keV) is measured to obtain two images of the subject, one mainly representing the concentrations of the low-Z elements, and another mainly of the intermediate-Z elements. DPA is used in both planar [2] and CT [6] modes to measure bone mineral content and bone mineral density. DPA with monochromatic x-rays produces images of much higher quality than those produced by wide-band sources. The algorithm that allows the two images to be generated is based on the ratio of the photoelectric to the Compton cross sections, which change differently with x-ray energy for those two groups of elements. Using the MECT system, the DPA image of the low-Z element group will emphasize the concentrations of H, C, N, O, and Na, and that of the intermediate-Z group will emphasize those of P, S, Cl, K, Ca, and Fe. In particular, the second group includes the neurologically important elements K and Ca, abnormal brain-tissue concentrations of which may reveal disorders such as ischemia and incipient infarction [7-9].

A.3 K-edge Subtraction (KES) CT

The 33.169 keV K-edge of the contrast element iodine is energetic enough to allow KES imaging of humans [3]. The method utilizes the 5.6-fold rise in the photoelectric absorption cross section at the iodine K-edge. KES of iodine with synchrotron-produced monochromatic x-rays has been used for transvenous coronary angiography of humans at the Stanford Synchrotron Radiation Laboratory (SSRL) [10-12], and at the NSLS [13]. KES CT of iodine also has been used at the SSRL to image coronary arteries in an excised, inert, pig heart [14].

B. Advantages of Synchrotron Radiation for Use in Monochromatic CT

Synchrotron radiation has the following advantages for CT over rotating-anode x-ray tube sources [15]:

a) Synchrotron radiation is naturally collimated in the forward direction, providing an ideal geometry for efficient use of the beam on a monochromator crystal. The fan-shaped beam is ideal for CT imaging. Furthermore, the near-parallel beam geometry allows the detector to be placed far behind the subject with only a marginal increase in the detector's size, an advantage that can almost completely eliminate subject-to-detector scattering [16].

b) Using synchrotron radiation fluxes, especially from wigglers, the monochromator yields are much higher than those that can be obtained from a CT x-ray tube positioned at one meter distance from a monochromator (see Fig. 2 for comparisons).

c) Although the virtual beam source size of a synchrotron source (~0.75 mm FWHM horizontal width at X17) is comparable to that of an x-ray tube, the larger ratio of source-to-subject distance:subject-to-detector distance in a synchrotron CT compared to a conventional CT system makes the geometrical image blurring effect much smaller for a synchrotron CT.

d) The temporal fluctuations of the synchrotron x-ray energy spectrum are much smaller than those of x-ray tube spectra, which are caused by high-voltage ripple.

III. SYSTEM COMPONENTS

A. The National Synchrotron Light Source (NSLS)

The NSLS facility encompasses two electron storage rings dedicated to the production of the synchrotron radiation in the vacuum ultraviolet (VUV) and x-ray ranges [17]. The x-ray ring operates at 2.5 GeV with sixteen bending magnets, each with a strength of 1.2 Tesla. The maximum beam current is 250 mA, and the lifetime of the beam varies from 10 to 40 hours. The critical energy (i.e. the energy that divides the area under the synchrotron radiation power spectrum into two halves) of the x-ray spectra from the bending magnets is 5.0 keV.

B. The X17 Superconducting Wiggler Beamline

A wiggler is an insertion device in a synchrotron storage ring (i.e. a magnetic structure interposed between bending magnets) that produces a linear array of static, vertical magnetic fields with alternating polarities [18].

The X17 Superconducting Wiggler is one of five insertion devices currently installed in the x-ray ring. The magnetic structure contains 7 poles (5 with full-field intensity and 2 with half-field intensity) having a period length of 17.4 cm and a gap of 3.2 cm [19], so that the physical length of the wiggler is 70 cm. For calculations, this wiggler can be adequately modeled by six poles at full-field intensity. The wiggler was commissioned in 1990 at a field of 4.7 Tesla. When the projected field of 5.2 Tesla is reached, the wiggler will provide an x-ray spectrum with a critical energy of 22.2 keV (Fig. 2).

C. Monochromator Design

The monochromator is a two-crystal Bragg-Bragg fixed-exit device [20], using Si <220> reflections. The fixed-exit beam is necessary for CT to allow dual-energy imaging of a single slice without changing the height of the patient and/or the detector. The monochromator has been designed to operate from 20 to 100 keV, which is the energy range necessary for DPA with small and large samples, and for KES of iodine and perhaps of heavier elements. The design and operation of a

monochromator in the energy range beyond 20 keV is complicated by the high degree of parallelism required to keep the two monochromator crystals in alignment. The reflection widths of the perfect single crystal silicon elements are ~1 arcsecond at 20 keV. The monochromator will operate under ultra-high vacuum.

The monochromator is based on the Golovchenko, or boomerang design [21], in which the angular coupling of the two crystals keeps the crystals parallel to each other at all Bragg angles within the operative range. In addition, the change in the Bragg angle is coupled to the translational motion of the second crystal. This motion keeps the second crystal in line with the diffracted beam from the first crystal, and maintains a constant vertical offset between the input and output beams.

A major specification of DPA applications is that the energy switching time should be short (5 seconds in our design) to minimize the number of revolutions of the patient per slice. This constraint presents a challenge for the monochromator design. Two possible energy switching techniques are being considered. One is to use the fundamental energy as the lower energy and the first harmonic as the higher energy, that is, to have the second energy twice the first. In this way, there is no change in the Bragg angle and energy switching is obtained by second-crystal detuning and by K-edge filtering [22]. The second technique is to switch the Bragg angle between two different values, which requires a fast-moving mechanism with high stability.

Fig. 3 shows the monochromator. It was tested recently at the X17B1 beamline. The first crystal is water cooled. The fine angular adjustment of the second crystal in both the Bragg direction and the tilt direction was obtained by using two piezoelectric transducers [23]. In particular, the Bragg angle fine tuning, which is used to adjust the yields of the fundamental and harmonic reflections, should be done within a fraction of an arcsecond. Fig. 4 shows the rocking curves (i.e., monochromator throughput versus second-crystal Bragg angle with first crystal fixed), obtained with a 55 mm^2 beam, 22 mm wide and 2.5 mm high, and filtered with 3 mm Al. The ring current was 150 mA.

D. Detector Design

The first choice for the detector is a high-purity germanium (HPGe) strip detector. There have been substantial advancements in production of these detectors [24,25] and as a result, HPGe detectors have been used in emission and in transmission computed tomography [26-28]. The specifications for an HPGe linear array detector for the MECT Project will be: 0.5 mm strip width; 10 mm strip height; 6 mm detector depth; and 200 mm overall detector width. The advantages of the Ge strip detector over other detectors used in CT scanners are the large linear dynamic range of its signals, and its small photon detection threshold. Four 33 keV x-ray photons coincident on one element produces a detectable signal using the current-integration method. Furthermore, compared to Si(Li) strip detectors, germanium has a much higher x-ray stopping power because of its higher Z.

A prototype HPGe strip detector of 45 mm width (i.e. 90 detection elements) is being manufactured at the Lawrence Berkeley Laboratory. Fig. 5 shows the cryostat made for this detector. A Si(Li) strip detector, with 128 elements of 0.25 mm width each, provided by the Stanford/NSLS Angiography Project, is being used for preliminary tests and imaging. The final 400-element HPGe detector will be made either of a single crystal element of 200 mm width, or of three crystal elements of each 67 mm width each, if the technical problems of manufacturing a long crystal cannot be overcome.

E. Electronics System

The electronics system will be based on a current-integration technique that allows a large signal dynamic range (10^6:1) and high linearity, to make good use of the high quality of the input data. Different designs of electronic circuits are being considered [29,30]. To achieve this dynamic range in the Data Acquisition System (DAS), a 20-bit digital data word should be generated from the detector current at each integration interval. One technique under consideration uses a 16-bit analog-to-digital convertor (for constant response for all detector

channels), along with a precision amplifier in which the gain is switched dynamically among three levels, producing multiplexed, 16-bit precision data over a 20 bit dynamic range [30].

F. Patient Chair

The patient chair is a critical component of the system since it partly determines the degree of loss of image quality due to its wobble and to the patient's motion. Since an in-plane resolution of 0.5 mm is desired in the reconstructed image, a high degree of mechanical stability of the central, vertical rotation axis is desirable. However, the inevitable wobble of this axis can be tracked electrooptically using mirrors attached firmly to the patient's head. The vector representing the deviation of the observed rotation axis from the ideal central axis during each acquisition interval will be used to correct the observed data before the image reconstruction. The degree to which this correction can compensate for wobble will suggest criteria for the patient's immobility and for the rigidity of the axis of the patient chair.

G. Medical Research Facility

The X17B beamline, which occupies the central segment of the X17 at the NSLS, is shared between two experimental areas. The X17B1 facility is dedicated to material sciences research, and the X17B2 facility, further downstream, is dedicated to Synchrotron Medical Research Facility (SMERF) [31]. The Coronary Angiography Project, which started at the SSRL, has been commissioned also at the SMERF facility. SMERF has been redesigned to accommodate the MECT project also. Fig. 6 shows the schematic of the MECT System on the X17 beamline. The facility has an area of 1500 sq ft, including rooms for reception, fluoroscopy, imaging, data acquisition, and control. The safety system, which has been designed, approved, and clinically tested for the Angiography Project [32], will form the basis for the MECT Project safety system.

H. System Parameters and Expected System Performance

The patient will be scanned around 360° rather than 180° around to distribute the skin dose evenly around the head, and also to allow better correction for the center-of-rotation motion. Each scan will take 5 seconds, with 5 additional seconds for energy switching. The maximum patient skin dose will be 5 rad for the combined two scans. The thickness will be in the 1-mm to 5-mm range. The data will be acquired in a continuous mode, with an angular sampling step of 0.14°, which takes 2 msec of the total 5-second scan time. The source strength is such that, with no subject in place, two million 40 keV photons will be detected in each detector strip in every 2-msec interval.

Theoretical estimates for the sensitivity of the MECT system were carried out, using the dual-energy algorithm developed by Riederer and Mistretta [33]. In these concentrations, spherical lesions with different concentrations of potassium and iodine were modeled inside a spherical sphere filled with water that simulates the head. The calculations estimate that the detection threshold for DPA CT will be a 10% change in the normal potassium concentration of the brain, or a 0.3 mg/cm^3 accumulation of calcium in the brain, in a lesion of 5-mm diameter. For KES CT, a 0.1 mg/cm^3 concentration of iodine in a 3 mm-diameter lesion should be detectable with a precision of ±30%. These values show advantage over the conventional CT by about ten-fold.

IV. CLINICAL RESEARCH PLAN

The clinical research plans for the human studies will include the following:

a) Dual Photon Absorptiometry (DPA) CT

- lesion of ischemia or incipient infarction [7-9]
- atherosclerotic plaques [34]
- neurological disorders that alter the concentration of the intermediate-Z elements in the brain, either regionally or globally.

b) K-Edge Subtraction (KES) CT

- small tumors
- lumens of arteries in the head and neck
- arteriovenous malformations

A very important advantage of the DPA and KES CT over conventional CT should be its quantitative precision. The system is expected to be an excellent quantitative CT (QCT). This means that concentrations of low-Z and intermediate-Z elements can be compared accurately in different patients.

Clinical aspects of this project will be carried out in collaboration with Drs. A.B. Kantrowitz, P.L. Kornblith, and J.R. Moskal of the Albert Einstein College of Medicine, Bronx, NY; and Drs. H.L. Atkins, J.D. Fenstermacher, F.A. Henn, H.M. Kuan, C.T. Roque, and C.S. Patlak of the School of Medicine, State University of New York at Stony Brook.

ACKNOWLEDGMENTS

The authors wish to thank Drs. J.B. Hastings and D.P. Siddons for their assistance to this project, and C.A. Brite, A. Lenhard, M. Shleifer, and W.F. Stoeber for designing and constructing the monochromator and beamline components. The technical support of R. Greene is appreciated. The authors also wish to thank Dr. E. Rubenstein of the Stanford University Medical School for allowing us to use the Si(Li) strip detector and the electronics of the Angiography Project. Valuable comments by Drs. A.-M. Fauchet, H.M. Kuan, A.U. Luccio and A.D. Woodhead are appreciated. This research has been carried out with the support of U.S. Department of Energy under Contract No. DE-AC02-76CH00016, and has been reported, in part, at the Eleventh International Conference on the Application of Accelerators in Research and Industry, Denton, Texas; November 5-8, 1990.

REFERENCES

[1] Stonestrom JP, Alvarez RE, Macovski A. A framework for spectral artifact corrections in x-ray CT. IEEE Trans Biom Eng 1981; BME-28: 128-41.

[2] Peppler WW, Mazess RB. Total body bone mineral and lean body mass by dual-photon absorptiometry. Calcif Tissue Int 1981; 33: 353-9.

[3] Brody WR, Macovski A, Pelc NJ, Lehmann L, Joseph RA, Edelheit LS. Intravenous arteriography using scanned projection radiography. Radiol 1981; 141: 509-14.

[4] Coleman AJ, Sinclair M. A beam-hardening correction using dual-energy computed tomography. Phys Med Biol 1985; 30: 1251-56.

[5] Cann CE, Genant HK. Precise measurement of vertebral mineral content using computed tomography. J Comp Assisted Tom 1980; 4; 493-500.

[6] Genant HK, Block JE, Steiger P, Glueer CC, Smith R. Quantitative computed tomography in assessment of osteoporosis. Sem Nucl Med 1987; 17: 316-33.

[7] Mies G, Kloiber O, Drewes LR, Hossmann KA. Cerebral blood flow and regional potassium distribution during focal ischemia of gerbil brain. Ann Neurol 1984; 16: 232-7.

[8] Hansen AJ. Effects of anoxia on ion distribution in the brain. Physiol Rev 1985; 65: 101-48.

[9] Siesjo BK. Calcium and ischemic brain damage. Eur Neurol 1986; 25: 45-56.

[10] Rubenstein E, Hofstadter R, Zeman HD, Thompson AC, Otis JN, Brown GS, Giacomini JS, Gordon HJ, Kernoff RS, Harrison DC, Thomlinson W. Transvenous coronary angiography in humans using synchrotron radiation. In: Proc Natl Acad Sci USA 1986; 83: 9724-8.

[11] Thompson AC, Zeman HD, Thomlinson W, Rubenstein E, Kernoff RS, Hofstadter R, Giacomini JC, Gordon HJ, Brown GS. Imaging of coronary arteries using synchrotron radiation. Nucl Inst and Meth in Phys Res 1989; B40/41: 407-12.

[12] Rubenstein E, Giacomini JC, Gordon HJ, Thompson AC, Brown GS, Hofstadter R, Thomlinson W, Zeman HD. Synchrotron radiation coronary angiography with a dual-beam, dual-detector imaging system. Nucl Inst and Meth in Phys Res 1990; A291: 80-5.

[13] Thomlinson W, private communication.

[14] Thompson AC, Llacer J, Campbell Finman L, Hughes EB, Otis JN, Wilson S, Zeman HD. Computed tomography using synchrotron radiation. Nucl Instr and Meth in Phys Res 1984; 222: 319-23.

[15] Grodzins L. Optimum energies for x-ray transmission tomography of small samples. Nucl Instr and Meth 1983; 206: 541-5.

[16] Johns PC, Yaffe M. Scattered radiation in fan beam imaging systems. Med Phys 1982; 9: 231-9.

[17] van Steenbergen A, and NSLS Staff. The National Synchrotron Light Source basic design and project status. Nucl Inst and Meth 1980; 172: 25-32.

[18] Hsieh H, Krinsky S, Luccio A, van Steenbergen A. Design of a 6 Tesla wiggler for the National Synchrotron Light Source. IEEE Trans Nucl Sci 1981; NS-28: 3292-4.

[19] Thomlinson W, Chapman D, Gmür N, Lazarz N. The superconducting wiggler beamport at the National Synchrotron Light Source. Nucl Inst and Meth 1988; A266: 226-33.

[20] Cowan PL, Hastings JB, Jach T, Kirkland JP. A UHV compatible two-crystal monochromator for synchrotron radiation. Nucl Instr and Meth 1983; 208: 349-53.

[21] Golovchenko JA, Levesque RA, Cowan PL. X-ray monochromator system for use with synchrotron radiation sources. Rev Sci Instr 1981; 52: 509-16.

[22] Zeman HD, Dilmanian FA, Garrett RA, Berman LE, Chapman LD, Hastings JB, Oversluizen T, Siddons DP, Stojanoff V, Thomlinson WC. An X-ray monochromator for dual-energy computerized tomography using synchrotron radiation. Nucl Instr and Meth (In press. 1991).

[23] Oversluizen T, Stefan PM, Iarocci M. Practical notes on the construction and use of a UHV double-crystal monochromator for synchrotron radiation. Vacuum 1987; 37: 321-5.

[24] Luke PN. Gold-mask technique for fabricating segmented-electrode germanium detectors. IEEE Trans Nucl Sci 1984; NS-31: 312-5.

[25] Gutknecht D. Photomask technique for fabricating high purity germanium strip detectors. Nucl Instr and Meth in Phy Res 1990; A288: 13-8.

[26] Ortendahl DA, Kaufman L, Rowan W, Herfkens R, Price DC. High resolution emission computed tomography with a small germanium camera. IEEE Trans Nucl Sci 1980; NS-27: 459-62.

[27] Mauderli W, Fitzgerald LT. Rotating laminar emission camera with Ge-detector: Further developments. Med Phys 1987; 14: 1027-31.

[28] Hasegawa BH, Gingold EL, Reilly SM, Liew SC, Cann C. Decription of a simultaneous emission-transmission CT system. SPIE Medical Imaging IV: Image Formation 1990; 1231: 50-60.

[29] Nakamura M, Katz JE, Thompson AC. A multichannel, high linerarity current digitizer for digital subtraction angiography. IEEE Trans Nucl Sci 1988; NS-35: 205-8.

[30] Analogic, Peabody, MA

[31] Thomlinson W, Gmür N, Zeman HD, Otis JN, Hofstadter R, Thompson AC, Brown GS, Rubenstein E, Giacomini JC, Gordon HJ, Kernoff RS. The synchrotron radiation angiography program at the National Synchrotron Light Source. In: Synchrotron Radiation Applications to Digital Subtraction Angiography (SYRDA), Italian Physical Society Conference Proceedings, Vol. 10. E. Burattini and A. Rindi, Eds. 1988; pp 173-80.

[32] Gmür NF, Thomlinson W. Safety analysis report X17B2 beamline-synchrotron medical research facility (SMERF). BNL Report BNL-52205, Addendum, 1989.

[33] Riederer SJ, Mistretta CA. Selective iodine imaging using K-edge energies in computerized x-ray tomography. Med Phys 1977; 4: 474-81.

[34] Cunningham IA, Hobbs BB, Fenster A. A new system for quantitative arterial imaging and blood flow measurements. Invest Radiol 1986; 21: 465-71.

FIGURE CAPTIONS

Fig. 1. Schematic top view of the MECT System.

Fig. 2. X-ray flux curves from three wigglers in the United States: the X17 at the NSLS, the 6-Pole wiggler at Cornell High Energy Synchrotron Source (CHESS), and the 54-Pole wiggler at the Stanford Synchrotron Radiation Laboratory (SSRL). The flux values were obtained for the maximum ring current. An x-ray tube flux is shown for comparison.

Fig. 3. The two-crystal monochromator.

Fig. 4. The rocking curves of the monochromator.

Fig. 5. Cryostat for the HPGe detector.

Fig. 6. Schematic view of the MECT system at the X17 beamline.

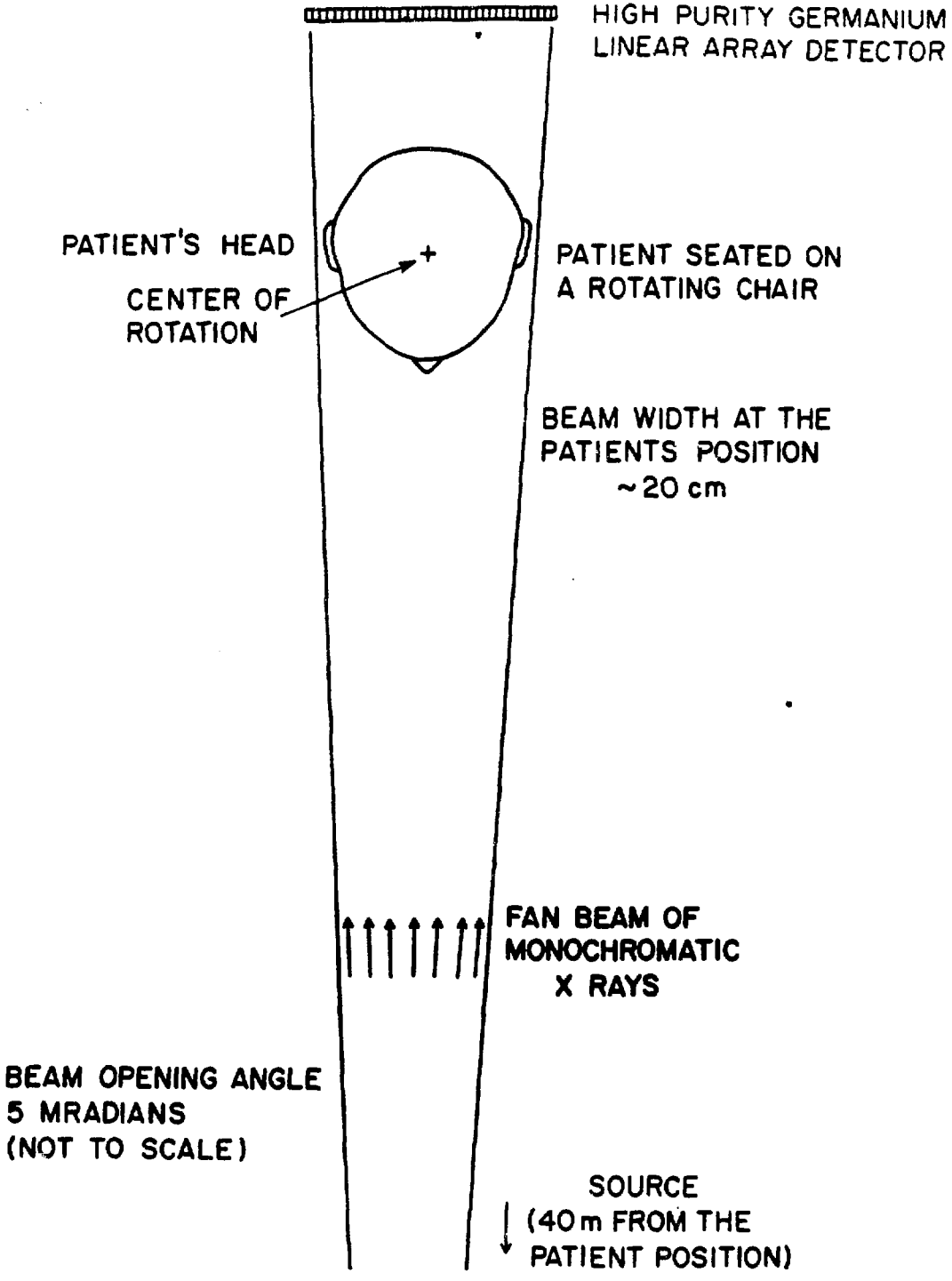
HIGH PURITY GERMANIUM
LINEAR ARRAY DETECTOR
PATIENT'S HEAD
CENTER OF
ROTATION
PATIENT SEATED ON
A ROTATING CHAIR
BEAM WIDTH AT THE
PATIENTS POSITION
~20 cm
FAN BEAM OF
MONOCHROMATIC
X RAYS
BEAM OPENING ANGLE
5 MRADIANS
(NOT TO SCALE)
SOURCE
(40 m FROM THE
PATIENT POSITION)

Figure 1

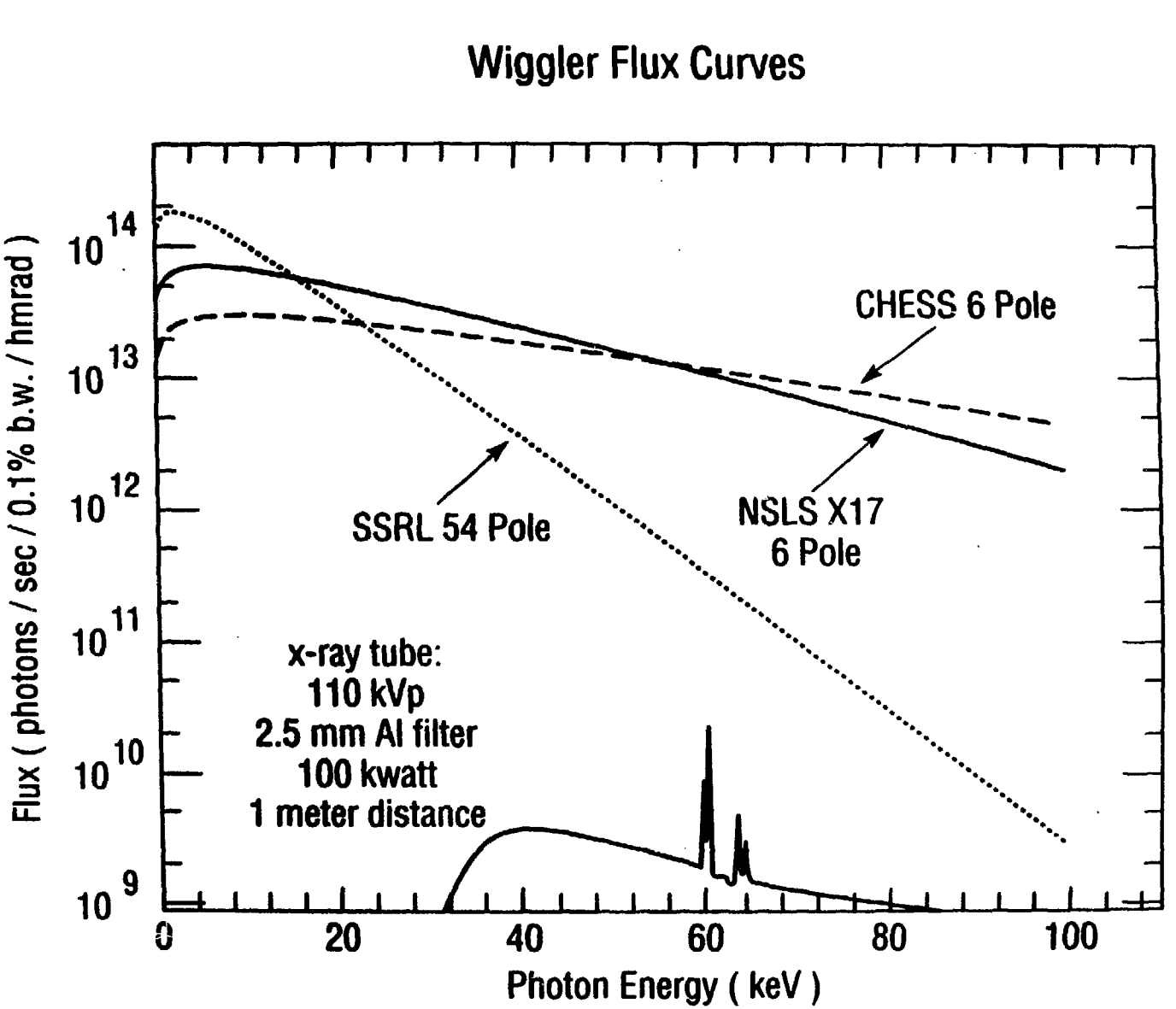
Wiggler Flux Curves
Flux (photons / sec / 0.1% b.w. / hmrad)
10^{14}
10^{13}
10^{12}
10^{11}
10^{10}
10^{9}
CHESS 6 Pole
SSRL 54 Pole
NSLS X17
6 Pole
x-ray tube:
110 kVp
2.5 mm Al filter
100 kwatt
1 meter distance
0
20
40
60
80
100
Photon Energy (keV)

Figure 2

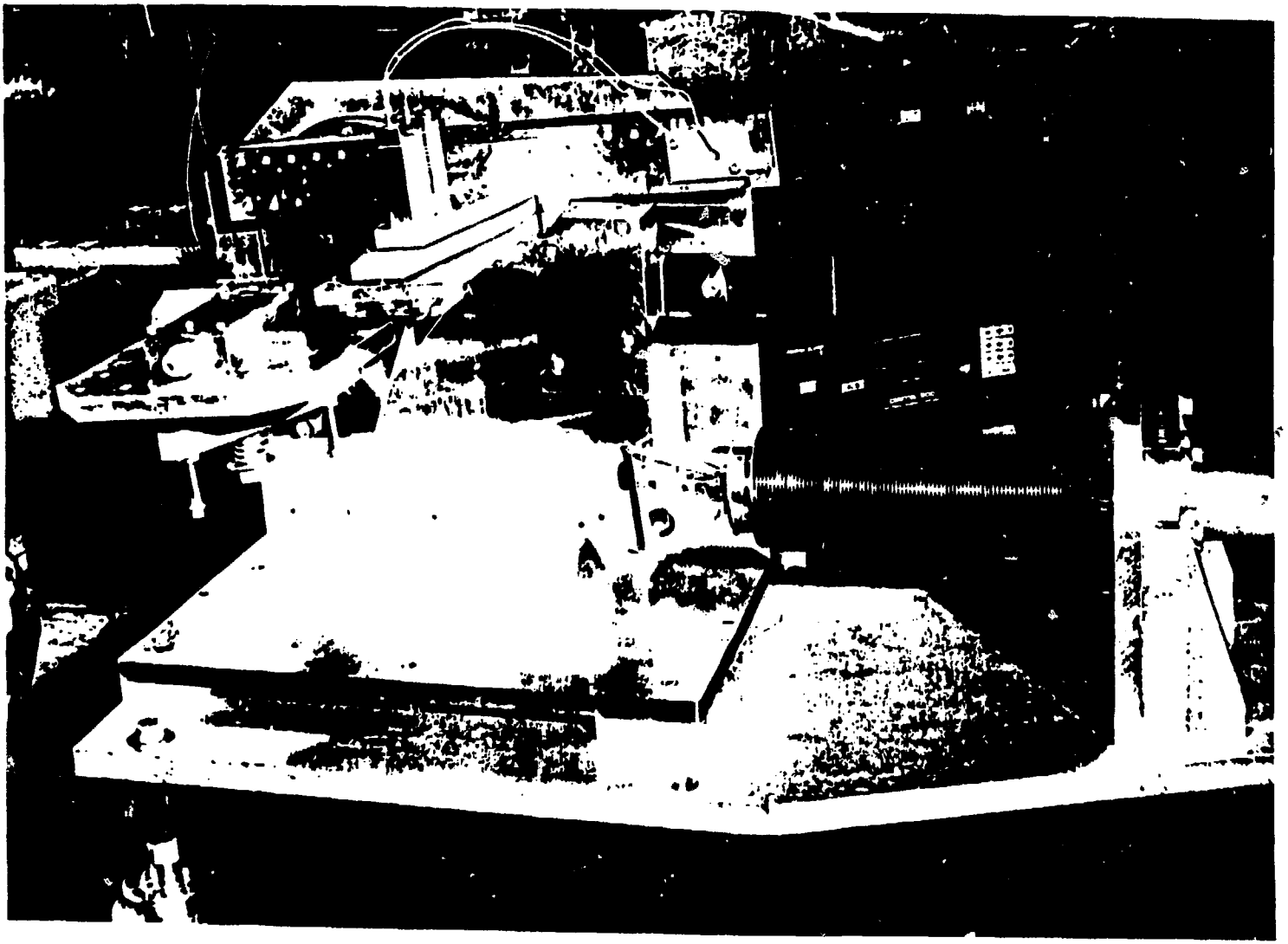

Figure 3

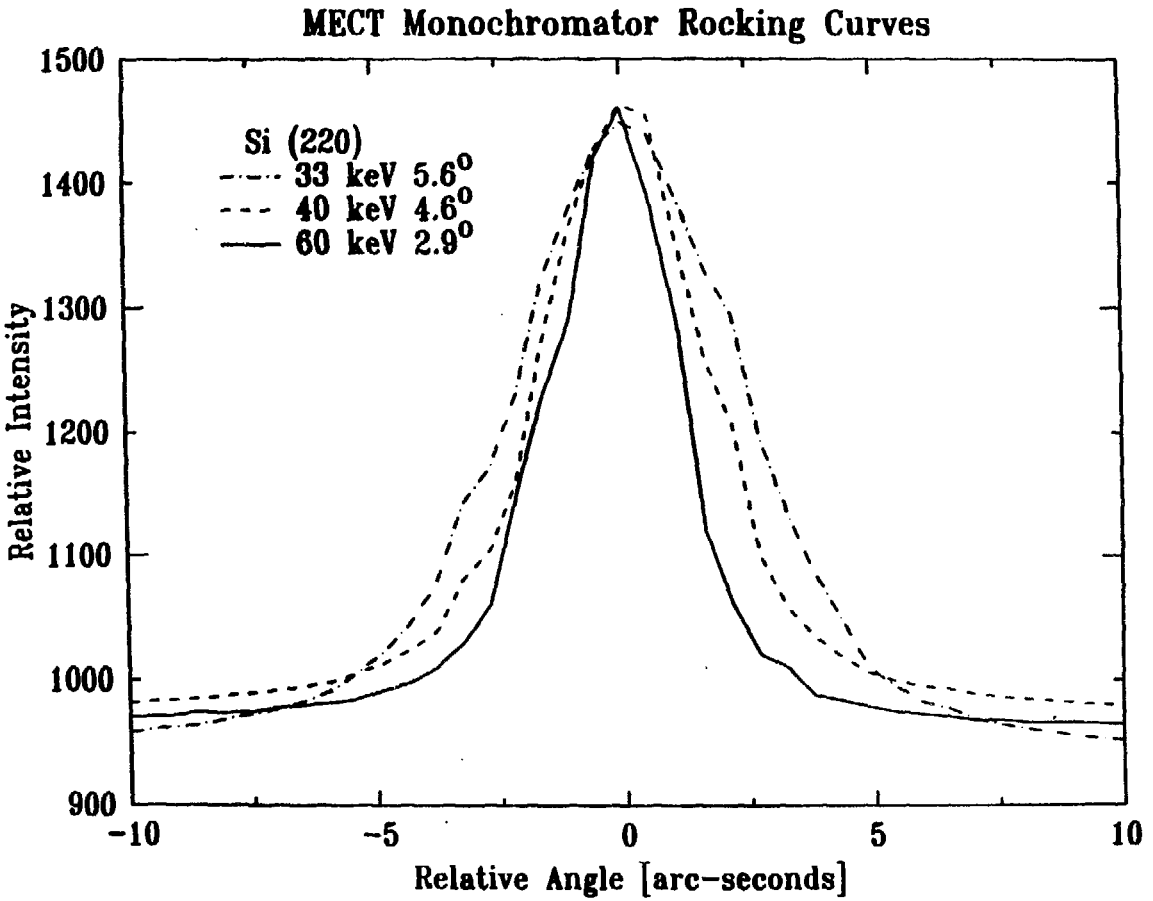
MECT Monochromator Rocking Curves
Si (220)
33 keV 5.6°
40 keV 4.6°
60 keV 2.9°
Relative Intensity
1500
1400
1300
1200
1100
1000
900
−10
−5
0
5
10
Relative Angle [arc-seconds]

Figure 4

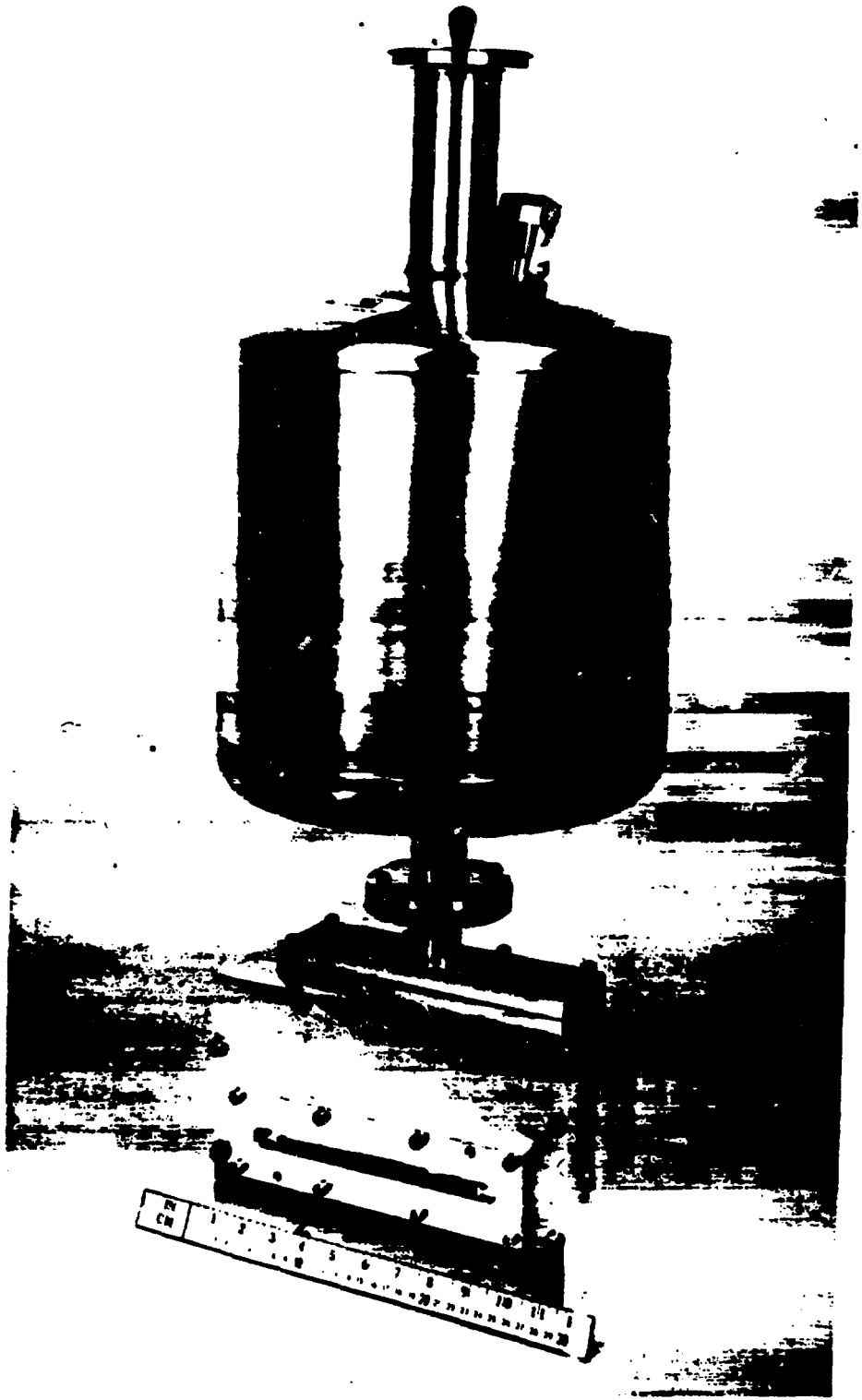

Figure 5

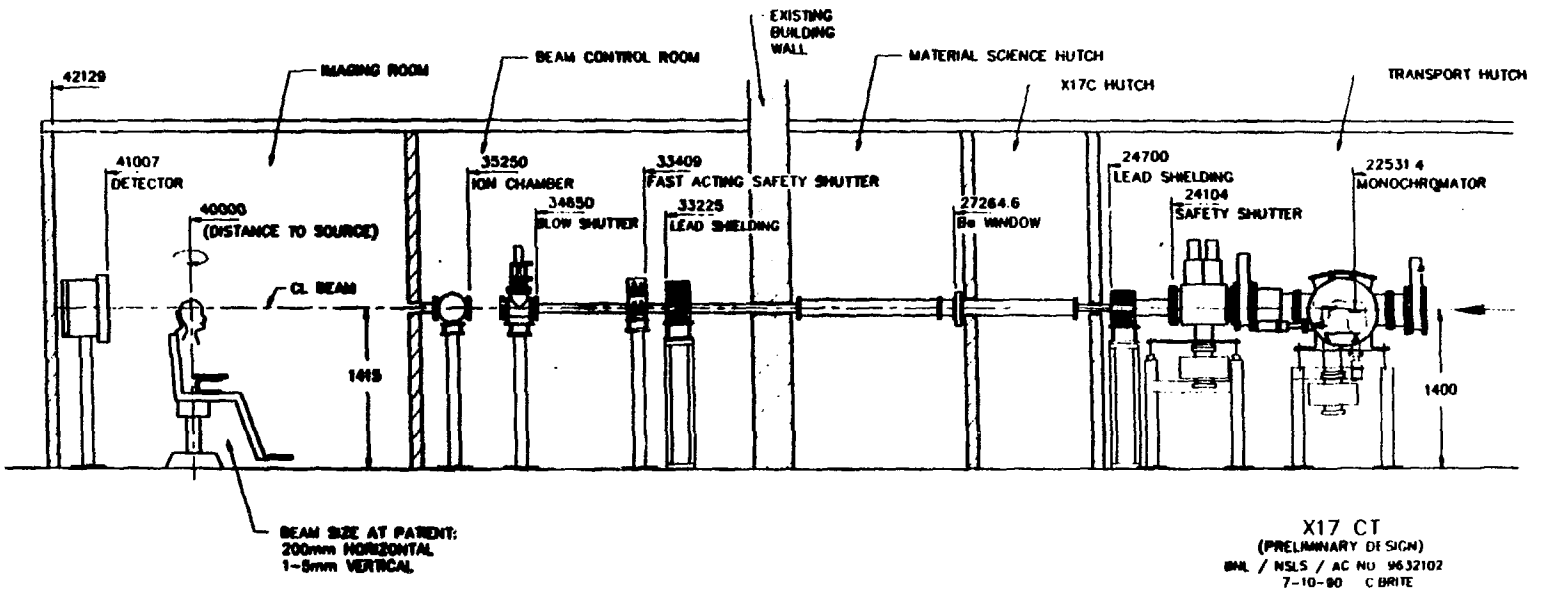
42129
IMAGING ROOM
BEAM CONTROL ROOM
EXISTING BUILDING WALL
MATERIAL SCIENCE HUTCH
X17C HUTCH
TRANSPORT HUTCH
41007
DETECTOR
40000
(DISTANCE TO SOURCE)
35250
ION CHAMBER
34850
SLOW SHUTTER
33409
FAST ACTING SAFETY SHUTTER
33225
LEAD SHIELDING
27264.6
Be WINDOW
24700
LEAD SHIELDING
24104
SAFETY SHUTTER
22531.4
MONOCHROMATOR
CL BEAM
1415
1400
BEAM SIZE AT PATIENT:
200mm HORIZONTAL
1-5mm VERTICAL
X17 CT
(PRELIMINARY DESIGN)
BNL / NSLS / AC NO 9632102
7-10-80 C BRITE

Figure 6